CrossMark
click for updates

# MHD MIXED CONVECTIVE HEAT AND MASS TRANSFER THROUGH A STRATIFIED NANOFLUID FLOW OVER A THERMAL RADIATIVE STRETCHING CYLINDER

**Srinivas Maripala**[1][†] --- **Kishan Naikoti**[2]

[1]*Department of mathematics, Sreenidhi Institute of Science and Technology, Hyderabad, Telangana India*
[2]*Departmnet of Mathematics, Osmania University, Hyderabad, Telangana, India*

## ABSTRACT

*The flow problem presented in this paper is to study the heat and mass transfer characteristics of a mixed convection nanofluid flow along a stretching cylinder embedded in a thermally stratified medium are numerically analyzed, with the thermal radiation effects. The governing boundary layer equations of continuity, momentum, energy and concentration are transformed into a set of ordinary differential equations with the help of suitable local similarity transformations. The coupled non-linear ordinary differential equations are solved by the implicit finite difference method along with the Thomas algorithm. The effect of various material parameters such as buoyancy parameter, solutal buoyancy parameter, Prandtl number, radiation parameter, Schmidt number, curvature parameter, magnetic parameter, stratification parameter, Brownian motion parameter and thermophoresis parameter on the velocity, temperature and concentration profiles are presented in graphs. Physical quantities such as skin friction coefficient, Nusselet number and Sherwood number are also computed.*

**Keywords:** Nano fluid, Thermal radiation, Thermal stratification, Mixed convection, Mass transfer, Stretching cylinder.

## Contribution/Originality

The primary contribution of this paper is finding that the effects of nanofluid on the heat and mass transfer characteristics of a mixed convection along a radiative stretching cylinder embedded in a thermal stratified medium. Aim of this paper is to develop a computational procedure.

† Corresponding author

## 1. INTRODUCTION

Choi [1] has first proposed the term nanofluid, which contains 1 to 100 nm sized particles. He has been verified that addition of nanoparticles in conventional base fluids appreciably enhanced the thermal conductivity. The study of convective heat transfer in nanofluids has achieved great success in various industrial applications, for example, hybrid-powered engines, in microelectronics, fuel cells,, nuclear reactors, transportations, biomedicine/pharmaceutical processes and pasteurization of food. In these processes, heat transfer takes place through some heat transfer devices; such as heat exchangers, evaporators, condensers and heat sinks. Increasing the heat transfer efficiency of these devices is desirable to minimize the space. Further in most of the heat transfer systems the working fluid is circulated by a pump, so the associated power consumption should be minimized [2]. A variety of nuclear reactor designs featured by enhanced safety and improved economics are being proposed by the nuclear power industry around the world to more realistically solve the future energy supply shortfall. In order to secure safety and economics, nanofluid coolants exhibiting improve thermal performance are being considered as a new key technology [3].

The study of boundary layer flow and heat transfer over an exponentially stretching cylinder has attracted many researchers due to its applications in fiber technology, flow meter design, piping and casting systems etc. Lin and Shih [4]; Lin and Shih [5] analyzed the laminar boundary layer and heat transfer along horizontally and vertically moving cylinders with constant velocity and found that the similarity solutions could not be obtained due to the curvature effect of the cylinder. Wang [6] investigated the steady flow of a viscous and incompressible fluid outside a stretching hollow cylinder in an ambient fluid at rest. Ishak, et al. [7] studied the flow and heat transfer of an incompressible electrically conducted viscous fluid outside of a stretching cylinder in the presence of a constant transverse magnetic field. Elbashbeshy, et al. [8] studied laminar boundary layer flow of an incompressible viscous fluid along a stretching horizontal cylinder embedded in a porous medium in the presence of a heat source or sink with suction/injection.

Mixed convection in porous media has many applications such as food processing and storage, geophysical system, metallurgy, fibrous insulation and underground disposal of nuclear waste [9]. Thermal conductivity of the conventional heat transfer fluids, for example water, is very low. Increasing thermal conductivity of the conventional fluids leads to improve the heat transfer of these fluids. Recently, nanofluids are introduced with enhanced thermal conductivity. A nanofluid is a suspension of nanoparticles in the base fluid. Because of the enhanced thermal conductivity, nanofluids are proposed for many industrial applications such as transportation, nuclear reactors and food [10, 11]. Cheng [12] evaluated mixed convection from a horizontal circular cylinder. Nield and Bejan [13], studied mixed convection about a horizontal cylinder in a porous medium. Khanafer and Vafai [14] investigated mixed convection heat transfer of a regular

41

fluid from a horizontal cylinder in porous media. Nazar, et al. [9] analyzed mixed convection of nanofluids from a horizontal circular cylinder embedded in a porous medium. In the work of him, the effect of copper, alumina and titanium oxide nanoparticles is evaluated. In the study of the effect of porosity and the thermal conductivity of porous medium on the effective thermal conductivity of the representative elementary. Srinivas and Kishan [15] studied the forced convection in unsteady magnatohydrodynamic boundary layer flow of a nanofluid over a permeable shrinking sheet in the presence of thermal radiation and chemical reaction. Macha and Kishan [16] investigated numerically with the MHD mixed convection boundary layer flow of heat and mass transfer stagnation-point flow of a non-Newtonian power-law nanofluid towards a stretching surface in the presence of thermal radiation and heat source/sink. Recently, Poornima and Bhaskar [17] studied the effect of the radiation on the heat and mass transfer flow, electrically conducting fluid past a stretching cylinder embedded in a thermally stratified porous medium. The present study of the heat and mass transfer characteristics of a mixed convection nanofluid flow along a radiating stretching cylinder embedded in a thermally stratified medium are numerically analyzed by the finite difference scheme along with the Thomas algorithm.

## 2. MATHEMATICAL ANALYSIS

A steady axi-symmetric mixed convection nanofluid flow of an incompressible viscous radiating fluid along a stretching cylinder embedded in a thermally stratified nanofluid-saturated medium of variable ambient temperature $T_\infty(x)$, where $T_w(x) > T_\infty(x)$ (heated surface), is considered. Figure-I, a uniform magnetic field intensity $B_0$ acts the radial direction, it is assumed that the effect of the induced magnetic field is negligible, which is valid when the magnetic Reynolds number is small. The fluid is considered to be a gray, absorbing emitting radiation, but non-scattering medium. The flow model and coordinate system are depicted as shown in Figure-I.
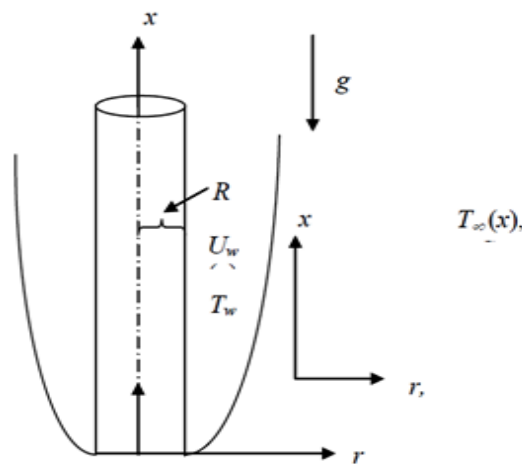


**Figure-I.** Flow model and coordinate system

The temperature and concentration of nanofluid outside the boundary layer are constant except that the influence of the density variation with temperature and concentration in the body force term (Boussinesq's approximation). Under the above assumptions the conservation equations of mass, momentum, energy and diffusion that govern the flow field [17] are

$$\frac{\partial(ru)}{\partial x} + \frac{\partial(rv)}{\partial y} = 0 \tag{1}$$

$$u\frac{\partial u}{\partial x} + v\frac{\partial u}{\partial r} = \frac{v}{r}\frac{\partial}{\partial r}\left(r\frac{\partial u}{\partial r}\right) + g\beta(T - T_\infty) + g\beta^*(C - C_\infty) - \frac{\sigma B_0^2}{\rho}u \tag{2}$$

$$u\frac{\partial T}{\partial x} + v\frac{\partial T}{\partial y} = \frac{k}{\rho C_p}\frac{1}{r}\frac{\partial}{\partial r}\left(r\frac{\partial T}{\partial r}\right) - \frac{1}{\rho C_p}\frac{1}{r}\frac{\partial(rq_r)}{\partial r} + \tau[D_B\frac{\partial C}{\partial r}\frac{\partial T}{\partial r} + \frac{D_T}{T_\infty}\left(\frac{\partial T}{\partial r}\right)^2] \tag{3}$$

$$u\frac{\partial C}{\partial x} + v\frac{\partial C}{\partial r} = \frac{D}{r}\frac{\partial}{\partial r}\left(r\frac{\partial C}{\partial r}\right) + \frac{D_T}{T_\infty}\frac{1}{r}\frac{\partial}{\partial r}\left(r\frac{\partial T}{\partial r}\right) \tag{4}$$

where $u$ and $v$ are the components of velocity in the $x$ and $r$ directions, respectively, $v = \mu/\rho$ is the kinematic viscosity, $\rho$ is the fluid density, $\mu$ is the coefficient of fluid viscosity, $k$ is the thermal conductivity of the fluid $T$ is the fluid temperature, $\sigma$ is the electrical conductivity of nanofluid and $B_0$ is the strength of the uniform magnetic field, $D_B$ is the Brownian diffusion coefficient, $D_T$ is the thermophoresis diffusion coefficient. $\tau$ is the ratio between the effective heat capacity of the nanoparticles ($\rho_{C_p}$) and heat capacity of the nanofluid ($\rho_{C_{nf}}$), i.e. $\tau = \rho_{C_p}/\rho_{C_{nf}}$. It is assumed that the convicting fluid and the medium are in local thermodynamic equilibrium.

The boundary conditions for the velocity, temperature and concentration of the problem are

$$u = U(x), \; v = 0, T = T_w(x), \; C = C_w \qquad \text{at } r = R \tag{5}$$
$$u \to 0, T \to T_\infty, \; C \to C_\infty \qquad \text{as } r \to \infty$$

where $R$ is the radius of the cylinder, $U(x) = U_0(x)/L$ is the stretching velocity, $T_w(x) = T_0 + b(x/L)$ is the prescribed surface temperature and $T_\infty(x) = T_0 + c(x/L)$ is the variable ambient temperature. Further, $U_0$ is the reference velocity, $T_0$ -the reference temperature and $L$ - the characteristic length. By using the Rosseland approximation [18] the radiative heat flux is given by

$$q_r = (-4\sigma_s/3k_e)\frac{\partial T^4}{\partial r} \tag{6}$$

Where $\sigma_s$ is the Stephen Boltzmann constant and $k_e$ - the mean absorption coefficient .It should be noted that by using the Rosseland approximation, the present analysis is limited to optically thick fluids. If the temperature differences within the flow are sufficiently small, then equation (5) can be linearized by expanding $T^4$ into the Taylor series about $T_\infty$ , which after neglecting higher order terms takes the form

$$T^4 \cong 4T_\infty^3 T - 3T_\infty^4 \tag{7}$$

Invoking equations (6) and (7), equation (3) can be modified as

$$u\frac{\partial T}{\partial x} + v\frac{\partial T}{\partial y} = \frac{k}{\rho C_p}\frac{1}{r}\frac{\partial}{\partial r}\left(r\frac{\partial T}{\partial r}\right) + \frac{16\sigma_s T_\infty^3}{3\rho C_p k_e}\frac{1}{r}\frac{\partial}{\partial r}\left(r\frac{\partial T}{\partial r}\right) + \tau[D_B\frac{\partial C}{\partial r}\frac{\partial T}{\partial r} + \frac{D_T}{T_\infty}\left(\frac{\partial T}{\partial r}\right)^2] \tag{8}$$

To get similarity solutions of equations (1) - (4) subject to the boundary conditions (5), we introduce the following similarity transformation:

$$\eta = \frac{r^2 - R^2}{2R}\sqrt{\frac{U}{vx}}, \quad \psi = (Uvx)^{\frac{1}{2}} R f(\eta), \quad \theta(\eta) = \frac{T - T_\infty}{T_w - T_0}, \quad \varphi(\eta) = \frac{C - C_\infty}{C_w - C_\infty}, \quad M = \frac{\sigma B_0^2 a^2}{4v\rho}$$

$$(9)$$

$$S = \frac{c}{b}, \quad \lambda = \frac{g\beta Lb}{U_0^2}, \quad Nb = \frac{g\beta^* L^2 (C_w - C_\infty)}{U_0^2}, \quad Nr = \frac{k_e k}{4\sigma T_\infty^3}, \quad A = \sqrt{\frac{vL}{U_0 R^2}} \tag{10}$$

Where $\psi$ is the stream function and the velocity components are defined as, $u = \frac{1}{r}\frac{\partial\psi}{\partial r}$,

$v = -\frac{1}{r}\frac{\partial\psi}{\partial x}$, which identically satisfies the continuity equation (1).

Using the above similarity transformations, equations (2) - (4) reduce to

$$(1 + 2A\eta)f''' + 2Af'' + ff'' - f'^2 + \lambda\theta + \delta\varphi - Mf' = 0 \tag{11}$$

$$(1 + \frac{4}{3Nr})\{(1 + 2A\eta)\theta'' + 2A\,\theta'\} + Pr(f\theta' - f'\theta - f'S) + Pr\eta\theta'(Nb\varphi' + Nt\theta') = 0 \tag{12}$$

$$(1 + 2A\eta)\varphi'' + 2A\,\varphi' + Scf\varphi' + \frac{Nt}{Nb}(\eta\,\theta'' + \theta') = 0 \tag{13}$$

The corresponding boundary conditions are

$$f' = 1, f = 0, \theta = 1 - S, \varphi = 1 \quad \text{at } \eta = 0 \tag{14}$$
$$f' \to 0, \quad \theta \to 0, \quad \varphi \to 0 \quad \text{as } \eta \to \infty$$

where prime denotes differentiation with respect to η, S is the stratification parameter, λ is the mixed convection parameter, $\delta$ is the volumetric concentration expansion , Nr is the radiation parameter A is the curvature parameter, Pr is Prandtl number, Le is Lewis number, Nb is Brownian motion parameter and Nt is thermophoresis parameter. We note that $S = 0$ is for an unstratified environment and $A = 0$ is for a flat plate. From technological point of view, it is of interest to calculate the shear stress, heat and mass fluxes which is given by

$$\tau_w = \mu(\frac{\partial u}{\partial r})_{r=R} = \frac{\mu U_0 x}{L}\sqrt{\frac{U_0}{vL}}f''(0)$$

$$q_w = -k(\frac{\partial T}{\partial r})_{r=R} = \frac{-kbx}{L}\sqrt{\frac{U_0}{vL}}\theta'(0) \qquad \text{and}$$

$$M_w = -D(\frac{\partial C}{\partial r})_{r=R} = -D\,(C_w - C_\infty)\sqrt{\frac{U_0}{vL}}\phi'(0)$$

In terms of non- dimensional quantities, the skin friction coefficient, Nusselt number and Sherwood number are given by

$$C_f = \frac{\tau_w}{\rho U_0^2/2} \Rightarrow \frac{1}{2}C_f Re_x^{1/2} = f''(0)$$

44

$$Nu_x = \frac{Lq_w}{kb} \Rightarrow Nu_x Re_x^{1/2} = -\theta'(0) \qquad\qquad\qquad \text{and}$$

$$Sh_x = \frac{xM_w}{D(C_w - C_\infty)} \Rightarrow \frac{Sh_x}{Re_x^{\frac{1}{2}}} = -\phi'(0)$$

## 3. NUMERICAL SOLUTION

The governing boundary layer and thermal layer (11)-(13) with boundary conditions (14) are coupled non-linear ordinary differential equations.

Applying the Quasi-linearization technique to the non-linear equation (11) and (12) we obtain as

$$\{1 + 2M\eta\}f'''[i] + \{2M + F[i]\}f''[i] - \{2F'[i]\}f'[i] + \{F''[i]\}f[i] = F[i]F''[i] - F'^2[i] - \lambda\theta[i] - \delta\phi[i] \qquad (15)$$

$$\left\{\left(1 + \frac{4}{3Nr}\right)(1 + 2M\eta)\right\}\theta''[i] \; +$$

$$\left\{2\left(1 + \frac{4}{3Nr}\right)M + Prf[i] + Pr\,\eta\,Nb\,\phi'[i] \; + 2Pr\,\eta\,Nt\,\phi'[i]\right\}\theta'[i] - \{Pr\,f'[i]\}\theta[i] =$$

$$\{S\,Pr\,f'[i] - Pr\,\eta\,Nt\theta1'^2[i]\} \qquad (16)$$

Where $F[i]$ is the n$^{\text{th}}$ iterative value of $f[i]$ which is a known function and $f[i]$ is unknown function at (n+1)$^{\text{th}}$ iteration. Here we set $\left|F - f\right| < 10^{-6}$.

Using an implicit finite difference scheme for the equation (15),(16) and (13), we obtain

$$A1[i]f[i+1] + B1[i]f[i] + C1[i]f[i-1] - D1[i]f[i-2] = E1[i]$$

$$A3[i]\theta[i+1] + B3[i]\theta[i] + C3[i]\theta[i-1] = E3[i]$$

$$A5[i]\phi[i+1] - B5[i]\phi[i] + C5[i]\phi[i-1] = E5[i]$$

Where

$$A1[i] = 2\{1 + 2M\eta\} + 2h\{2M + F[i]\} - 2h^2 F'[i]$$

$$B1[i] = -6\{1 + 2M\eta\} - 4h\{2M + F[i]\} + 2h^3 F''[i]$$

$$C1[i] = 6\{1 + 2M\eta\} + 2h\{2M + F[i]\} + 2h^2 F'[i]$$

$$D1[i] = 2\{1 + 2M\eta\}$$

$$E1[i] = 2h^3\{F[i]F''[i] - F'^2[i] - \lambda\theta[i] - \delta\phi[i]\}$$

$$A3[i] = 2\left(1 + \frac{4}{3Nr}\right)(1 + 2M\eta) + h\{2\left(1 + \frac{4}{3Nr}\right)M + Prf[i] + Pr\,\eta\,Nb\,\phi'[i]$$
$$+ 2Pr\,\eta\,Nt\,\phi'[i]\}$$

$$B3[i] = -4\left(1 + \frac{4}{3Nr}\right)(1 + 2M\eta)$$

$$- h\left\{2\left(1 + \frac{4}{3Nr}\right)M + Prf[i] + Pr\,\eta\,Nb\,\phi'[i] + 2Pr\,\eta\,Nt\,\phi'[i]\right\}$$

$$- 2h^2 Pr\,f'[i]$$

$$C3[i] = 2\left(1 + \frac{4}{3Nr}\right)(1 + 2M\eta)$$

$$E3[i] = 2h^3\{S\,Pr\,f'[i] - Pr\,\eta\,Nt\theta1'^2[i]\}$$

$$A5[i] = (1 + 2M\eta) + h(2M + Scf[i])$$

$$B5[i] = 2(1 + 2M\eta) + h(2M + Scf[i])$$

$$C5[i] = (1 + 2M\eta)$$

$$E5[i] = \frac{-Nt}{Nb}\{h^2(\eta\theta''[i] + \theta'[i])\}$$

Here the step size taken as h = 0.05 is obtained the numerical solution and solved the algebraic system of equations by using an implicit finite difference scheme of Cranck -Nicklson method with Thomas algorithm and five decimal accuracy is the criterion for convergence.

**Table-I**. Values of $-\theta'(0)$, $f''(0)$ and $-\phi'(0)$ for different values of Nt, *Nb*, *Pr and A* with $\lambda = 0.1$, δ=0.1, Nr=1.0, S=0.0, Sc=0.1

| | | $-\theta'(0)$ | $f''(0)$ | $-\phi'(0)$ |
|---|---|---|---|---|
| | 0.3 | 0.42187 | −0.43170 | 2.81962 |
| | 0.5 | 0.43297 | −0.37333 | 2.96866 |
| Nt | 1.0 | 0.45462 | −0.29950 | 3.16633 |
| | 0.3 | 0.42187 | −0.43170 | 2.81962 |
| | 0.5 | 0.43345 | −0.3191 | 2.93226 |
| Nb | 1.0 | 0.44561 | −0.2101 | 2.98209 |
| | 0.72 | 0.42187 | −0.43170 | 2.81962 |
| | 2.0 | 0.42380 | −0.38250 | 2.25579 |
| Pr | 3.0 | 0.42545 | −0.29450 | 2.38523 |
| | 1.0 | 0.60140 | -1.61724 | 0.83258 |
| | 3.0 | 0.41344 | −0.41314 | 2.01824 |
| A | 5.0 | 1.67862 | −0.50174 | 2.12550 |

## 4. RESULTS

The non-linear boundary value problem given by equations (11)–(13) and boundary conditions (14) has been solved by using the implicit finite difference scheme of Cranck-Nicklson type has been employed. The system of equations are reduced to tri-diagonal system of equations which are solved by the Thomas algorithm. The results have been carried out for various flow parameters such as buoyancy parameter $\lambda$, solutal buoyancy parameter $\delta$, Prandtl number *Pr*, Radiation parameter *Nr*, Schmidt number *Sc*, curvature parameter *A*, magnetic parameter *M*, stratification parameter *S*, Brownian motion parameter *Nb* and thermophoresis parameter *Nt* on

velocity, temperature and concentration fields are presented graphically in Figs.1 - 10. Here the value of $Pr$ is chosen as 0.71, which corresponds to air. The other parameters are chosen arbitrarily. Table-I presents the numerical values of the skin friction coefficient, Nusselt number and Sherwood number for various values of governing parameters. Table-I, it is observed that the skin friction coefficient, Nusselt number and Sherwood numbers are increased for both the cases Brownian motion parameter $Nb$ and thermophoresis parameter $Nt$ increases. The Prandtl number $Pr$ decreases the values of skin friction coefficient $f''(0)$, Nusselt number $-\theta'(0)$ and the Sherwood number $-\phi'(0)$ values increases. The curvature parameter $A$ decrease the values of Nusselt number and Sherwood number and increases the values of skin friction parameter.

Figures 1(a) - (c) represent the effect of curvature parameter A on the velocity, temperature and concentration. Physically $A = 0$ signifies the cylinder's outer surface behaves like a flat surface. It means as $A \rightarrow 1$, the viscosity effect reduces due to contact area of surface with fluid tends to the tangential position. From Figure1 (a), it is noticed that the effect of curvature parameter $A$ on the velocity field. In this case, nearer to the boundary layer, the velocity profiles decreases and reverse phenomenon observed far away from the boundary layer. Similar trend is observed for both the temperature and concentration i.e., initially both temperature and concentration and then they increase. The thermal buoyancy parameter $\lambda$ effects are shown in Figure 2(a)–(c). The effect of the thermal buoyancy parameter $\lambda$ on the velocity is presented in Fig.2(a). It is the fact that the positive buoyancy force acts like a favorable pressure gradient and hence accelerates the velocity of the fluid in the boundary layer. This results in higher velocity as $\lambda$ increases. Fig.2(b). illustrates the temperature profiles for different values of the thermal buoyancy parameter. It is observed that as the thermal buoyancy parameter increases, the temperature decreases. The concentration profiles for different values of the thermal buoyancy parameter λ are depicted in Fig. 2(c). It is noticed that the concentration decreases, as the thermal buoyancy parameter increases. The effect of the solutal buoyancy parameter δ on the velocity, temperature and concentration is shown in Figs.3 (a) − (c). With an increase in the solutal buoyancy parameter δ, the velocity increases while the temperature and the concentration decrease.

Figure 4(a)-(c) depicts the effect of Schmidt number $Sc$ on velocity, temperature and concentration profiles. It is observed that the velocity, temperature and species concentration decreases with the increases in Schmidt number $Sc$. physically this shows that an increase in $Sc$ causes a decrease in the molecular diffusion $D$. It is observed from Figure 5(a) - (c), that an increase in magnetic parameter $M$ leads to a decrease in velocity profiles. The velocity boundary layer thickness becomes thinner as $M$ increases. This is due to the fact that applications of magnetic field to an electrically conductivity fluid produce a drag-like force called Lorentz force. This force causes reduction in the fluid velocity. The thermal boundary layer thickness increases with the increasing the magnetic parameter $M$ has shown in figure 5(b). The reason for this

behavior is that the Lorentz force increases the temperature. The concentration profiles are increased with the increase of magnetic field parameter *M* is observed from Figure 5(c).

Figure 6(a)-(c) illustrate that the effect of Prandtl number *Pr* on velocity, temperature and concentration profiles. Prandtl number values decrease the velocity profiles, when it increases.

Fig.6 (b).depicts the effect of the Prandtl number *Pr* on the temperature. It is observed that as the Prandtl number *Pr* increases, the temperature decreases. If *Pr* is small (< 1), then the thermal diffusion occurs at a greater rate than the momentum diffusion and therefore the heat conduction is more effective than the convection. Conversely, if *Pr* is large (> 1), the momentum diffuses at a greater rate than the thermal diffusion and the convection is more effective than the conduction. Concentration profiles are increased with the increase of Prandtl number *Pr*, is observed from the Figure 6(c).The thermophoresis parameter *Nt* effects on Temperature and concentration profiles are illustrated through the graphs 7(a)-(b). It is observed that the thermophoresis parameter *Nt* leads to increase the temperature profiles and nanoparticle concentration. The effect of Brownian motion parameter *Nb* is to display on temperature and concentration profiles in figure 8(a) - 8(b). It is noticed that the temperature in the boundary layer increases and the nanoparticle concentration decreases with increase of Brownian motion parameter *Nb*.

The temperature profiles for different values of the radiation parameter *Nr* are illustrated in Fig.9. It is noticed that as the radiation parameter *Nr* increases, the temperature decreases. This is due to the fact that the divergence of the radiative heat flux increases as $\rho C p$ decreases, which in turn increases the rate of the radiative heat, transferred to the fluid. Therefore heat is able to diffuse away from the stretching cylinder causing the fluid temperature to decrease. The influence of the stratification parameter *S* on temperature profiles is shown in Fig.10. The thermal boundary layer thickness decreases with an increase in the stratification parameter *S*. Due to stratification, the temperature in the boundary layer decreases.
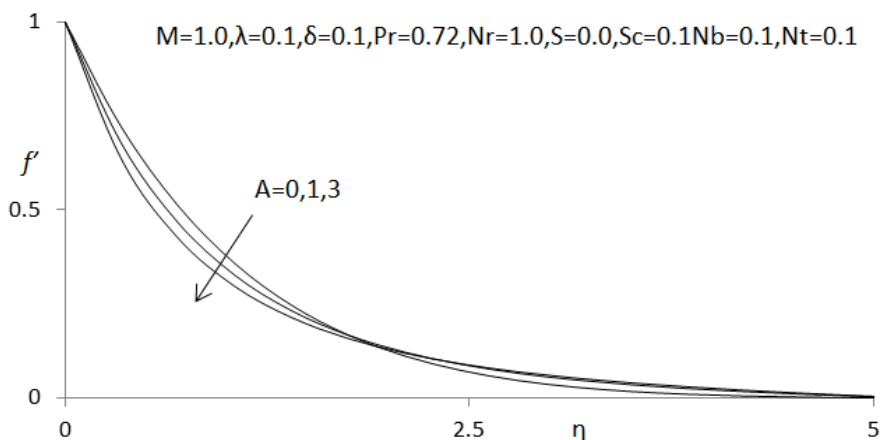


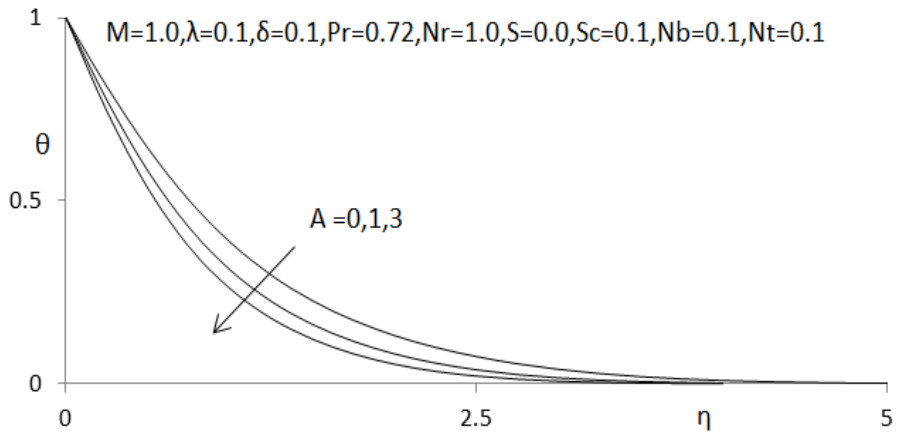**Fig–1(a).**Velocity profiles for different values of A

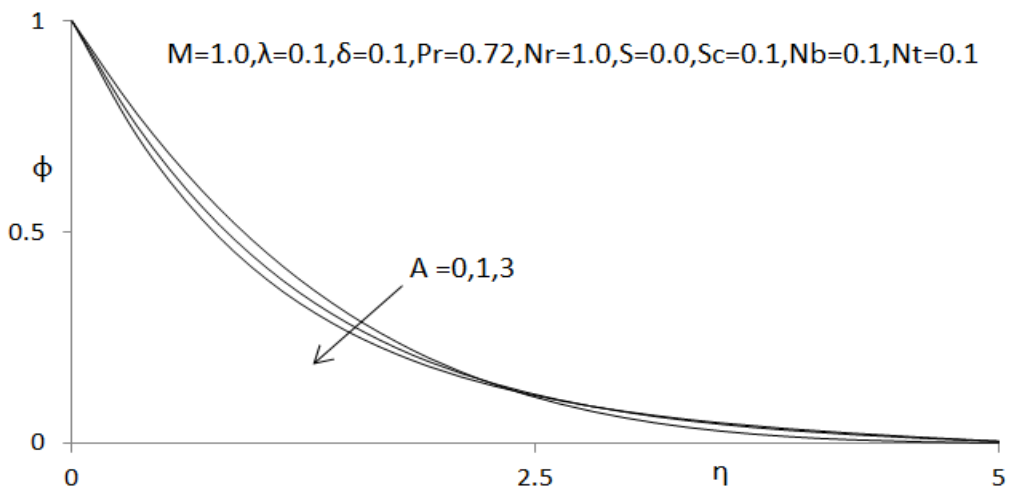**Fig-1(b).** Temperature profiles for different values of A



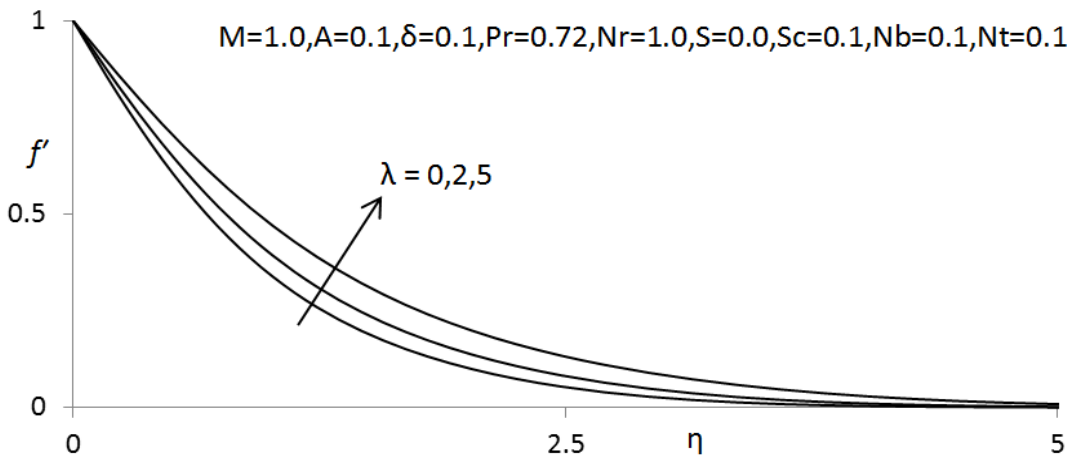**Fig-1(c).** Concentration profiles for different values of A



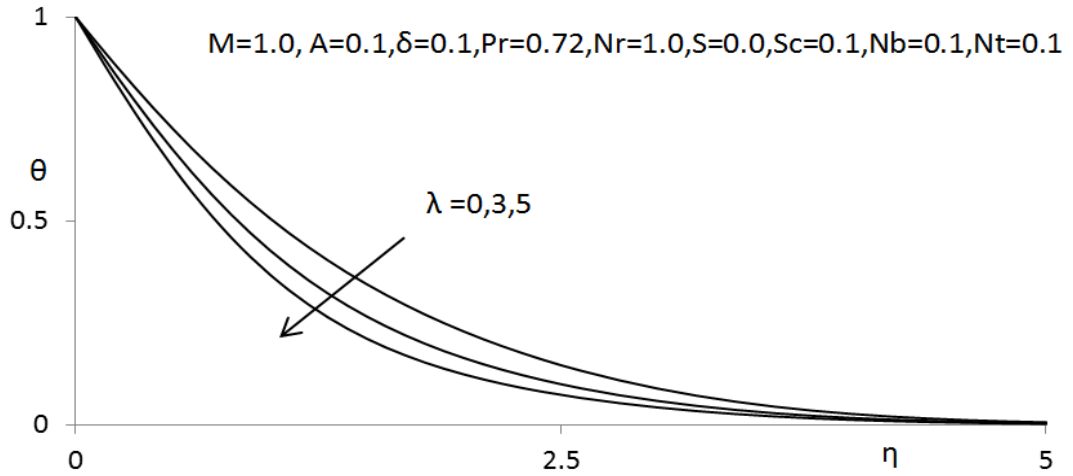**Fig-2(a).**Velocity profiles for different values of λ

49

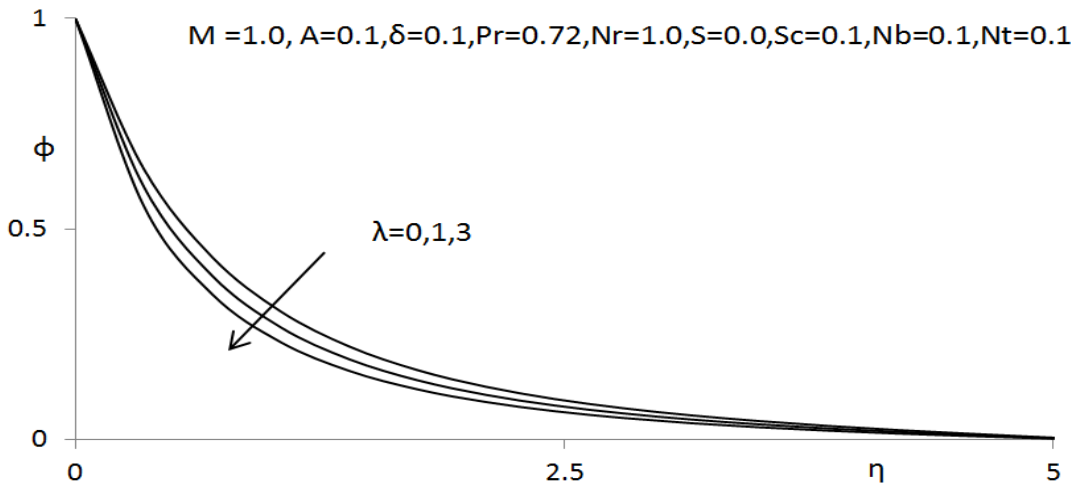**Fig-2(b).** Temperature profiles for different values of $\lambda$



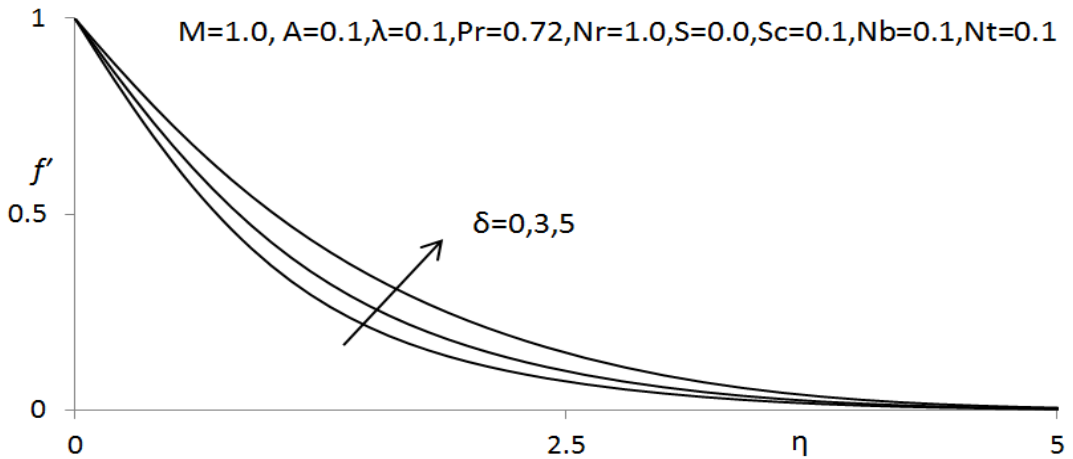**Fig-2(c).** Concentration profiles for different values of $\lambda$



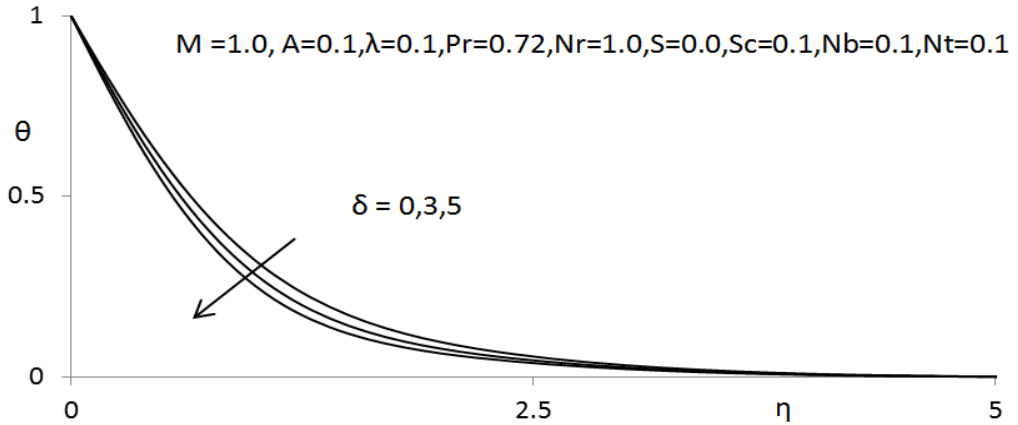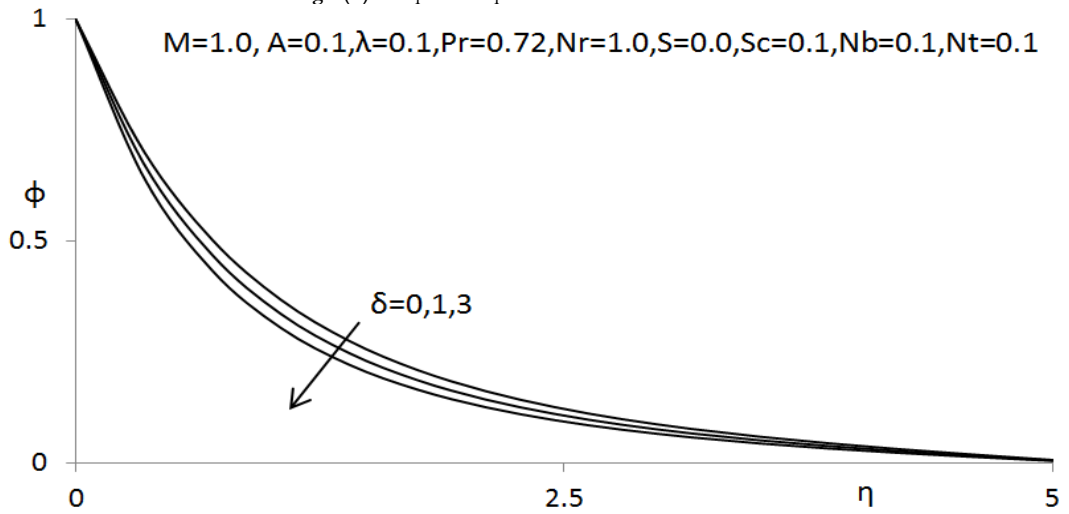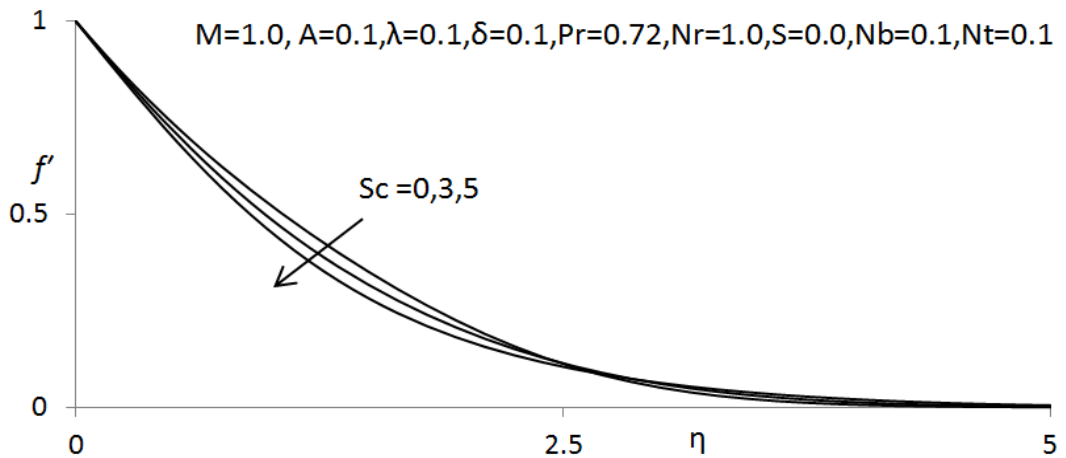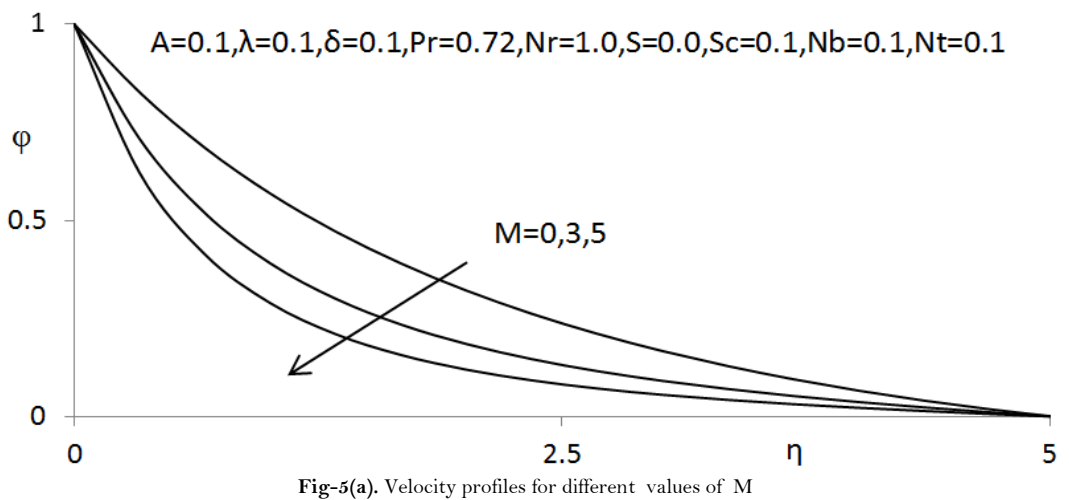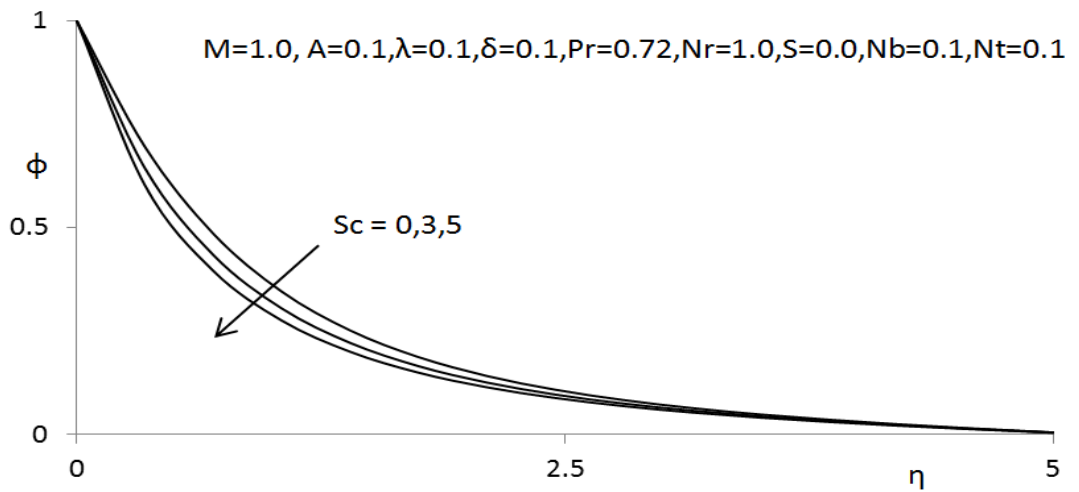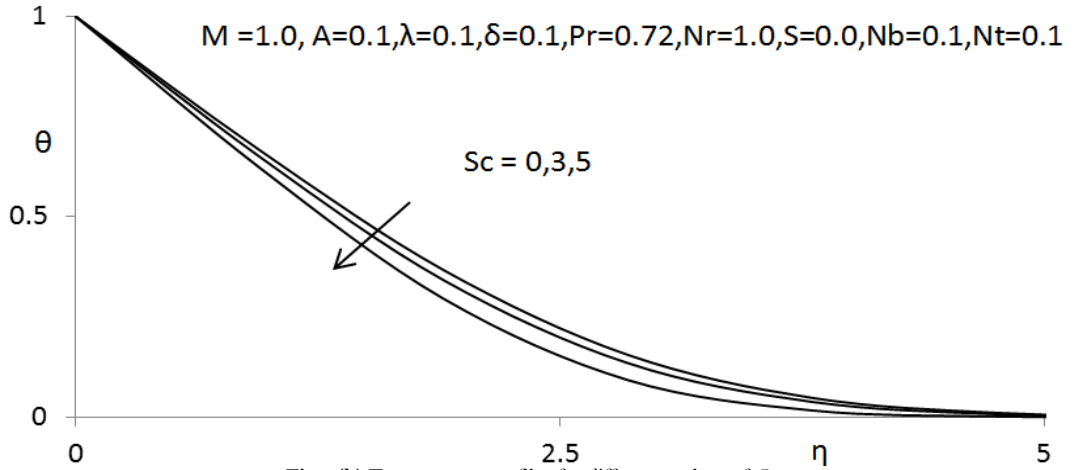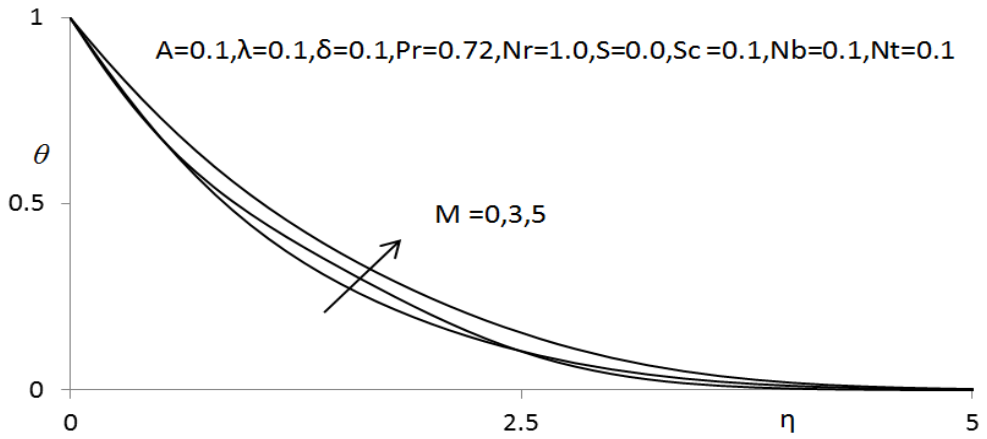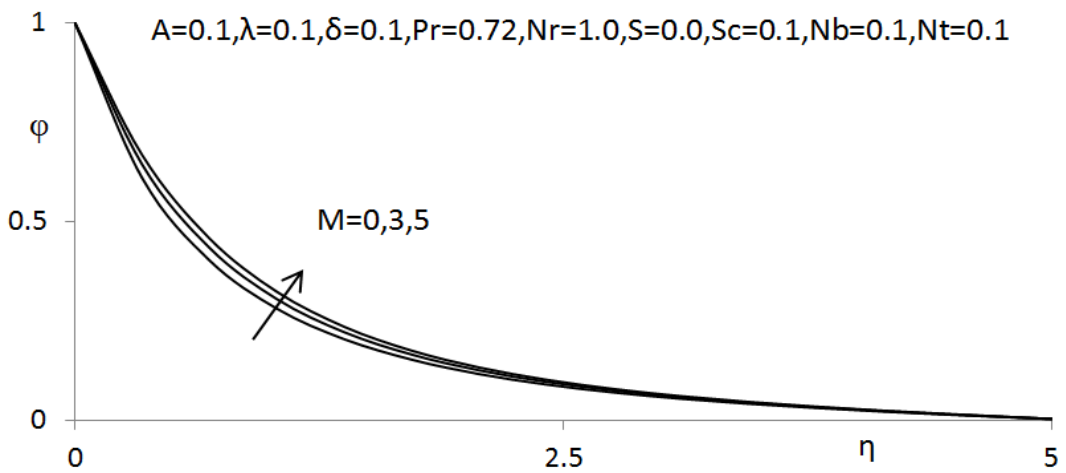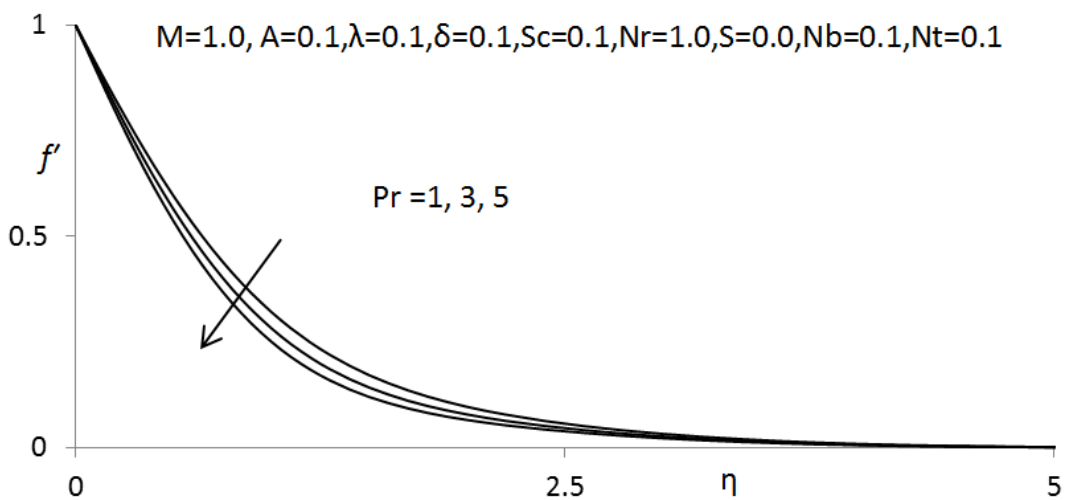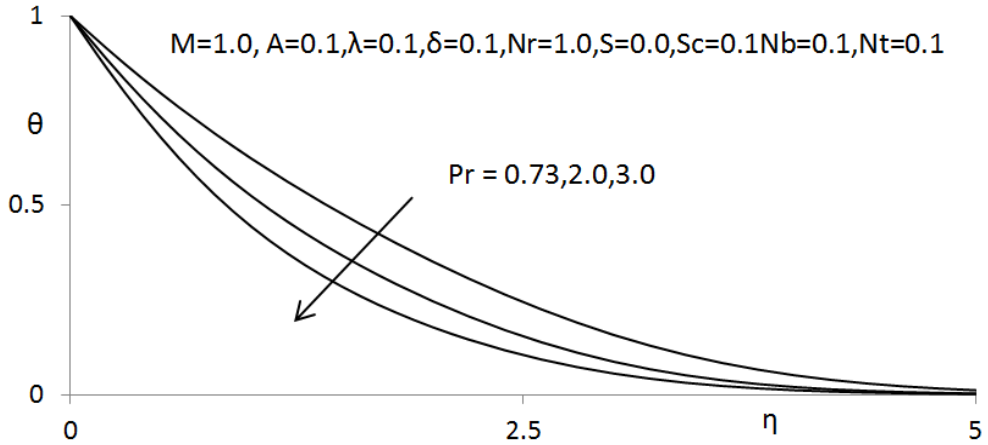**Fig-3(a).** Velocity profiles for different values of $\delta$

M =1.0, A=0.1,λ=0.1,Pr=0.72,Nr=1.0,S=0.0,Sc=0.1,Nb=0.1,Nt=0.1

$\delta = 0,3,5$

**Fig-3(b).**Temperature profiles for different values of δ



M=1.0, A=0.1,λ=0.1,Pr=0.72,Nr=1.0,S=0.0,Sc=0.1,Nb=0.1,Nt=0.1

$\delta=0,1,3$

**Fig-3(c).** Concentration profiles for different values of δ



M=1.0, A=0.1,λ=0.1,δ=0.1,Pr=0.72,Nr=1.0,S=0.0,Nb=0.1,Nt=0.1

Sc =0,3,5

**Fig-4(a).** Velocity profiles for different values of Sc

51

M =1.0, A=0.1,λ=0.1,δ=0.1,Pr=0.72,Nr=1.0,S=0.0,Nb=0.1,Nt=0.1

Sc = 0,3,5

**Fig-4(b).**Temperature profiles for different values of Sc

M=1.0, A=0.1,λ=0.1,δ=0.1,Pr=0.72,Nr=1.0,S=0.0,Nb=0.1,Nt=0.1

Sc = 0,3,5

**Fig-4(c).** Concentration profiles for different values of Sc

A=0.1,λ=0.1,δ=0.1,Pr=0.72,Nr=1.0,S=0.0,Sc=0.1,Nb=0.1,Nt=0.1

M=0,3,5

**Fig-5(a).** Velocity profiles for different values of M

A=0.1,λ=0.1,δ=0.1,Pr=0.72,Nr=1.0,S=0.0,Sc =0.1,Nb=0.1,Nt=0.1

M =0,3,5

**Fig-5(b).** Temperature profiles for different values of M

A=0.1,λ=0.1,δ=0.1,Pr=0.72,Nr=1.0,S=0.0,Sc=0.1,Nb=0.1,Nt=0.1

M=0,3,5

**Fig-5(c).** Concentration profiles for different values of M

M=1.0, A=0.1,λ=0.1,δ=0.1,Sc=0.1,Nr=1.0,S=0.0,Nb=0.1,Nt=0.1

Pr =1, 3, 5

**Fig-6(a).** Velocity profiles for different values of Pr

**Fig-6(b).**Temperature profiles for different values of Pr
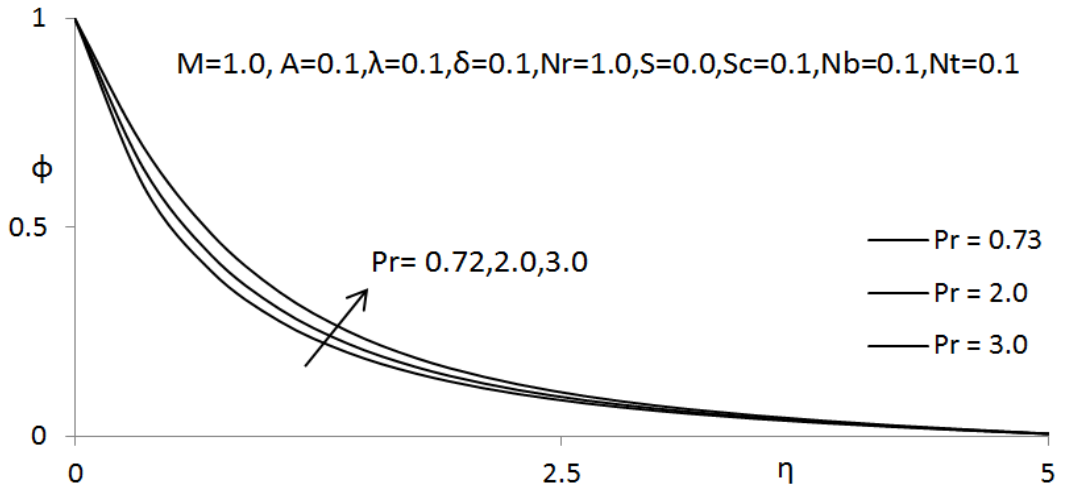


**Fig-6(c).** Concentration profiles for different values of Pr
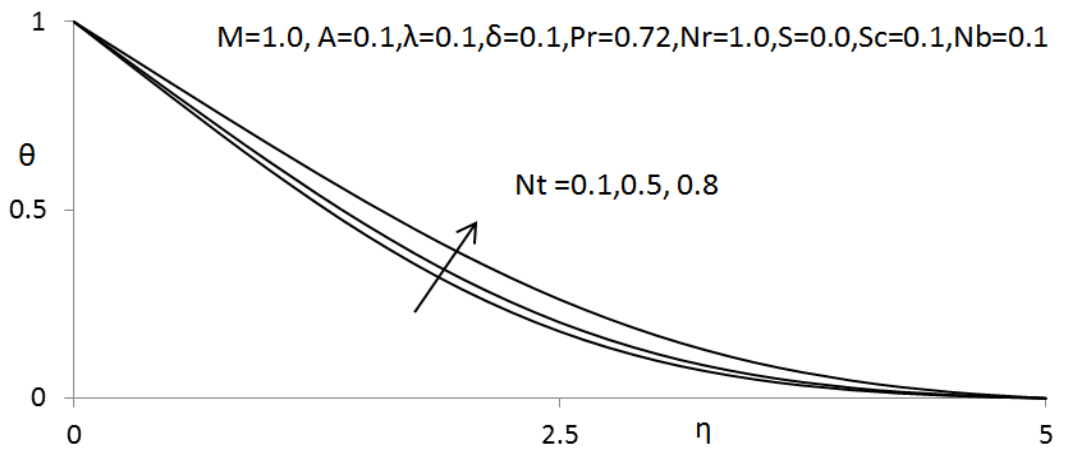

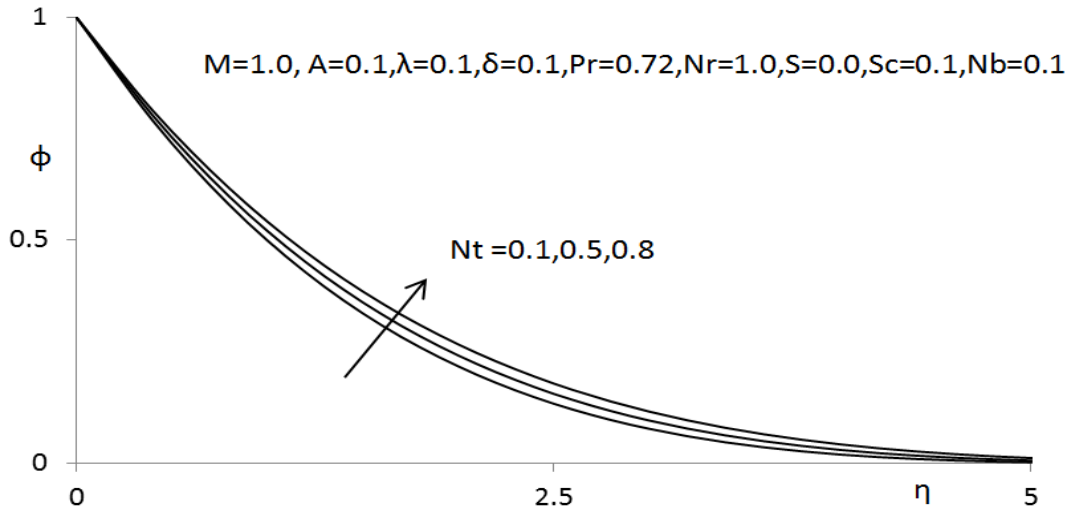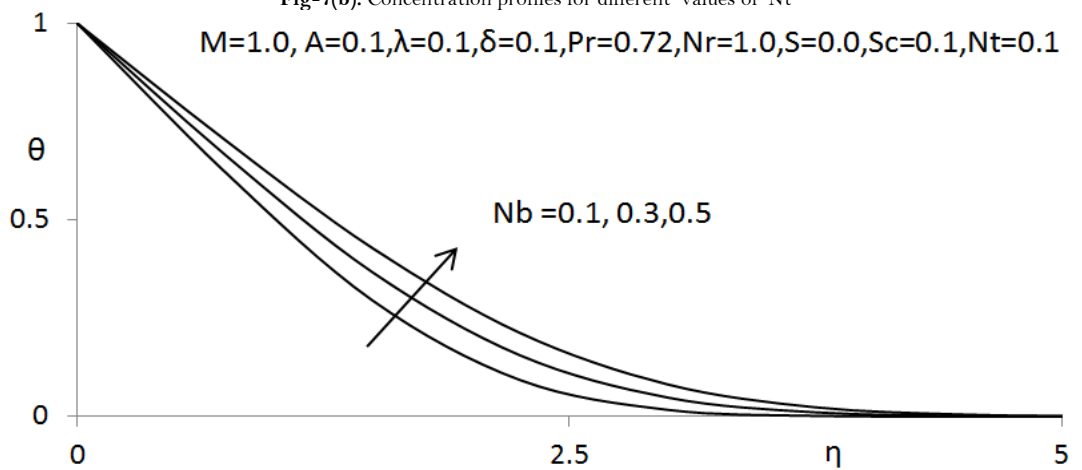
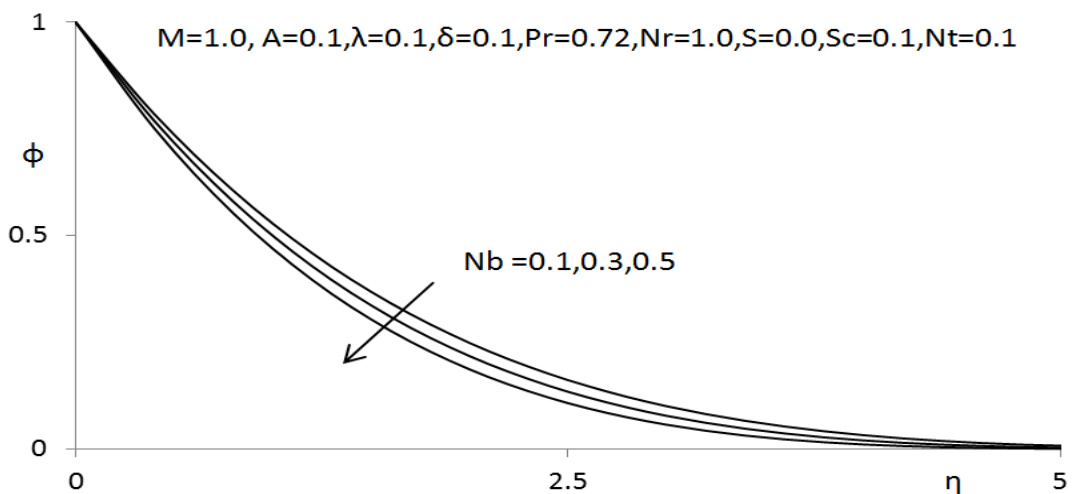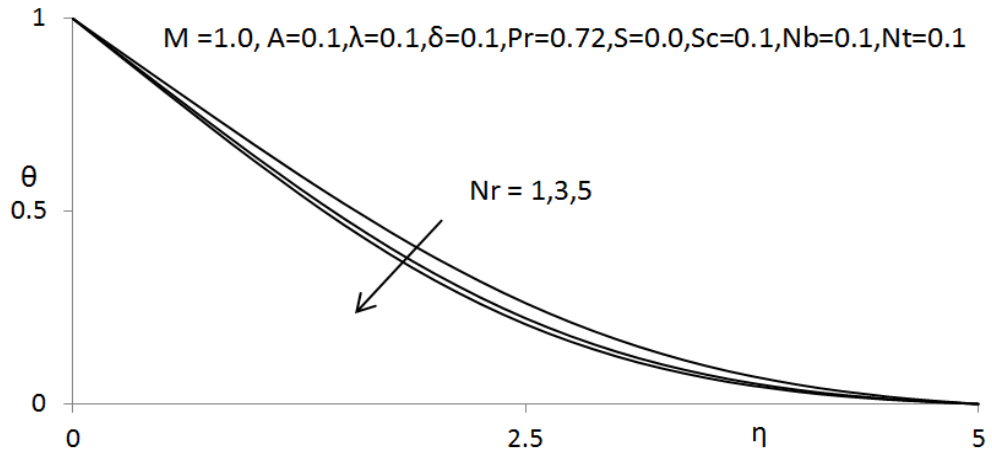**Fig-7(a).**Temparature profiles for different values of Nt

M=1.0, A=0.1,λ=0.1,δ=0.1,Pr=0.72,Nr=1.0,S=0.0,Sc=0.1,Nb=0.1

Nt =0.1,0.5,0.8

**Fig-7(b).** Concentration profiles for different values of Nt



M=1.0, A=0.1,λ=0.1,δ=0.1,Pr=0.72,Nr=1.0,S=0.0,Sc=0.1,Nt=0.1

Nb =0.1, 0.3,0.5

**Fig-8(a).**Temperature profiles for different values of Nb



M=1.0, A=0.1,λ=0.1,δ=0.1,Pr=0.72,Nr=1.0,S=0.0,Sc=0.1,Nt=0.1

Nb =0.1,0.3,0.5

**Fig-8(b).** Concentration profiles for different values of Nb

**Fig-9.** Temparature profiles for different values of Nr
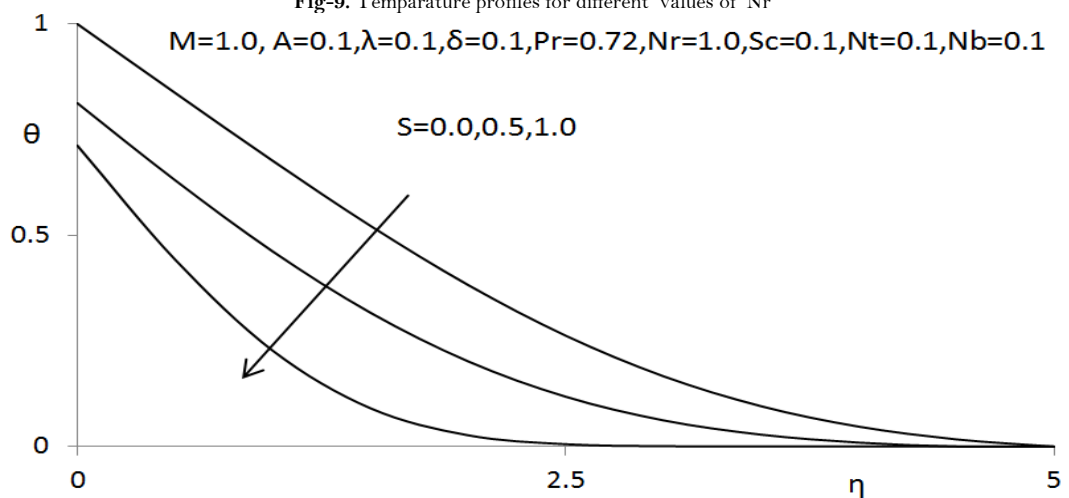


**Fig-10.** Temparature profiles for different values of S

## REFERENCES

[1]     S. U. S. Choi, "Enhancing thermal conductivity of fluids with nanoparticles," presented at the The Proceedings of the ASME International Mechanical Engineering Congress and Exposition, ASME, FED 231/MD, USA, 1995.

[2]     S. Ozernic, S. Kakac, and A. G. Yazicioglu, "Enhanced thermal conductivity ofnano fluids: A state of the art review," *Microfluid. Nanofluid*, vol. 8, pp. 145–170, 2012.

[3]     R. Kandasamy, P. Loganathan, and P. P. Arasu, "Scaling group transformation for MHD boundary layer flow of a nanofluid past a vertical stretching surface in thepresence of suction and injection," *Nuclear Eng. Design*, vol. 241, pp. 2053–2059, 2011.

[4]     C. R. Lin and Y. P. Shih, "Laminar boundary layer heat transfer alongstatic and moving cylinder," *J. Chin. Inst. Eng.*, vol. 3, pp. 73 −79, 1980.

[5]     C. R. Lin and Y. P. Shih, "Buoyancy effects on the laminar boundarylayer heat transfer along vertically moving cylinder," *J. Chin. Inst. Eng.*, vol. 4, pp. 45 − 51, 1981.

[6]     C. Y. Wang, "Fluid flow due to a stretching cylinder," *Phys. Fluids*, vol. 31, pp. 466–468, 1988.

[7]     A. Ishak, R. Nazar, and I. Pop, "Magnetohydrodynamic (MHD) flow andheat transfer due to a stretching cylinder," *Energy Convers Manag.*, vol. 49, pp. 3265 − 3269, 2008.

[8]     E. M. A. Elbashbeshy, T. G. Emam, M. S. El − Azab, and K. M. Abdelgaber, "Laminarboundary layer flow along a stretching horizontal cylinderembedded in a porous medium in the presence of a heat source or sinkwith suction/injection," *International Journal of Energy & Technology*, vol. 4, pp. 1 − 6, 2012.

[9]     R. Nazar, L. Tham, I. Pop, and D. Ingham, "Mixed convection boundary layer flow from a horizontalcircular cylinder embedded in a porous medium filled with a nanofluid," *Transport in Porous Media*, vol. 86, pp. 517–536, 2011.

[10]    R. Saidur, K. Leong, and H. Mohammad, "A review on applications and challenges of nanofluids," *Renewable and Sustainable Energy Reviews*, vol. 15, pp. 1646-1668, 2011.

[11]    X. Q. Wang and A. S. Mujumdar, "Heat transfer characteristics of nanofluids: A review," *International Journal of Thermal Sciences*, vol. 46, pp. 1–19, 2007.

[12]    P. Cheng, "Mixed convection about a horizontal cylinder and sphere in a fluid-saturated porousmedium," *International Journal of Heat and Mass Transfer*, vol. 25, pp. 1245–1246, 1982.

[13]    D. A. Nield and A. Bejan, *Convection in porous media*. New York, USA: Springer, 2013.

[14]    K. Khanafer and K. Vafai, "A critical synthesis of thermophysical characteristics of nanofluids," *International Journal of Heat and Mass Transfer*, vol. 54, pp. 4410–4428, 2011.

[15]    M. Srinivas and N. Kishan, "Unsteady MHD flow and heat transfer of nanofluid over a permeable shrinking sheet with thermal radiation and chemical reaction," *American Journal of Engineering Research*, vol. 4, pp. 68-79, n.d.

[16]    M. Macha and N. Kishan, "Magnetohydrodynamic mixed convection stagination-point flow of a power-law non-newtonian nanofluid towards a stretching surface with radiation and heat source/sink," *Journal of Fluids*, Hindawi Publishing Corporation, vol. 2015, pp. 1-14, 2015.

[17]    T. Poornima and R. N. Bhaskar, "Mixed convection heat and mass transfer flow along a stretching cylinder in a thermally stratified medium with thermal radiation effects," *Journal of Global Research in Mathematical Archives*, vol. 1, pp. 72-82, 2015.

[18]    M. Q. Brewster, *Thermal radiative transfer properties*. New York, USA: Wiley, 1992.